An Evaluation of Analog and Numerical Techniques for Unsteady Heat Transfer Measurement with Thin-Film Gauges in Transient Facilities

William K. George
William J. Rae
Scott H. Woodward
Calspan-UB Research Center, Buffalo, New York

■ The importance of frequency response considerations in the use of thin-film gauges for unsteady heat transfer measurements in transient facilities is considered, and methods for evaluating it are proposed. A departure frequency response function is introduced and illustrated by an existing analog circuit. A Fresnel integral temperature which possesses the essential features of the film temperature in transient facilities is introduced and is used to evaluate two numerical algorithms. Finally, criteria are proposed for the use of finite-difference algorithms for the calculation of the unsteady heat flux from a sampled temperature signal.

Keywords: *thin-film gauge, unsteady heat transfer, transient environments, heat flux measurement*

INTRODUCTION

The use of thin-film gauges for heat transfer measurement in transient facilities has been well established over the past 30 years (Vidal [1]; see Schultz and Jones [2] for an excellent review). Until recently, attention was focused either on relatively simple flows (such as the passage of a shock wave) or on attempts to measure "mean" heat transfer rates on gas turbine blades under quasi-steady conditions. In both types of experiments, attention was focused on capturing the rise in temperature and mean heat flux, and the fluctuations due to periodic flow disturbances or turbulence were of little interest. In recent years, there has been considerable interest in extending the thin-film technique to the measurement of fluctuating heat transfer rates in transient experiments, especially with regard to gas turbine applications (Dunn and Holt [3]; Dunn et al [4, 5]; Doorly and Oldfield [6]). All of these experiments used an analog circuit, hereafter referred to as the Q-meter, to convert the surface temperature measured by the thin-film gauges to heat flux signals. The Q-meter was originally developed in the late 1950s (Skinner [7]; Meyer [8]) and was redesigned by Oldfield et al [9] to the wide-band analog used in this report. While this circuit has the advantage of directly presenting an analog voltage proportional to heat transfer rate, its design is based on the assumption of constant thermal properties of the substrate, a condition violated in some experiments. Moreover, the Q-meter, although a considerable improvement over the original designs, has a bandwidth substantially lower than that of the gauge itself.

An alternative to the Q-meter is to directly record the surface temperatures and then calculate the heat flux numerically from either the one-dimensional heat transfer equation or an analytic solution to it. One of the most successful examples of the latter is the numerical algorithm of Cook and Felderman [10] and Cook [11], which assumed constant thermal properties. Dunn et al [5] attempted to include variable thermal properties by numerically solving the governing equations using the thin-film surface temperature data as input. Prior to the present work, a portion of which was reported by Dunn et al [5], there appears to have been no attempt to analyze the ability of these numerical techniques to resolve fluctuating heat transfer rates.

The purpose of this paper is to present a detailed evaluation of the frequency response of both analog and numerical approaches to the determination of fluctuating heat transfer rates from the output of thin-film gauges in transient environments. The amplitude and phase errors are determined, and their effect on simulated signals is assessed.

THE PRINCIPLE AND GOVERNING EQUATIONS

Transient heat transfer measurements with thin-film gauges depend primarily on the applicability of one-dimensional heat conduction as shown in Fig. 1 so that the process can be described by the one-dimensional equation

$$\rho C \frac{\partial T}{\partial t} = \frac{\partial}{\partial x}\left(k \frac{\partial T}{\partial x}\right) \tag{1}$$

subject to the surface condition

$$\dot{q}(0, T) = -k \left.\frac{\partial T}{\partial x}\right|_{x=0} \tag{2}$$

Address correspondence to Professor W. K. George, Mechanical & Aerospace Engineering, University at Buffalo, SUNY, 340 Jarvis Hall, Amherst NY 14260.

Experimental Thermal and Fluid Science 1991; 4:333–342

0894-1777/91/$3.50

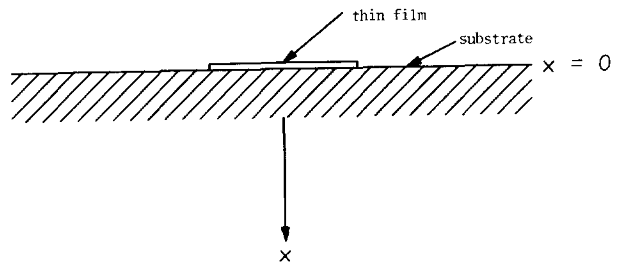

Figure 1. Coordinate system for Eq. (1).

For constant thermal properties, this equation can be solved analytically using Laplace or Fourier transform techniques. If $\hat{T}(0,f)$ and $\hat{q}(0,f)$ are the Fourier transforms of the surface temperature and heat flux, respectively, then

$$\hat{q}(0,f) = \sqrt{\rho C k}\,\sqrt{j2\pi f}\,\hat{T}(0,f) \tag{3}$$

from which it follows that the moduli and phases are related by

$$|\hat{q}(0,f)| = \sqrt{\rho C k}\,\sqrt{2\pi f}\,|\hat{T}(0,f)| \tag{4}$$

and

$$\angle\,\hat{q}(0,f) = \angle\,\hat{T}(0,f) + 45^\circ \tag{5}$$

AMPLITUDE AND PHASE RESPONSE

The ideal analog Q-meter would be one which duplicates the response characteristics of Eqs. (3)-(5) over the frequency range of interest. Any deviation from this ideal characteristic will result in a distortion of the unsteady heat transfer signal.

That this is indeed the case can be seen by viewing the Q-meter as a linear circuit as shown in Fig. 2*a*. For such systems the Fourier transform of the output is simply the Fourier transform of the input multiplied by the frequency response function of the system.* Thus if $\hat{e}_i(f)$ and $\hat{e}_{oi}(f)$ represent the input and output to this ideal system,

$$\hat{e}_{oi}(f) = H_{\text{ideal}}(f)\,e_i(f) \tag{6}$$

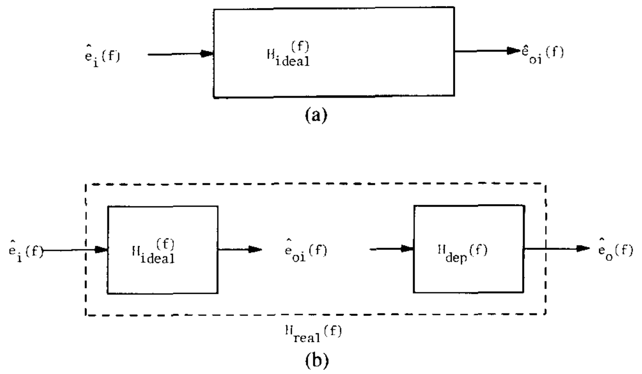

Figure 2. (a) Schematic of ideal linear system. (b) Schematic of real linear system showing departure from ideal.

* The frequency response function of a system is the Fourier transform of the impulse response function of that system.

The ideal frequency response function for a Q-meter would be (to within a factor dependent on the thermal properties of the substrate)

$$H_{\text{ideal}}(f) = \sqrt{j2\pi f} \tag{7}$$

In practice, circuits are never ideal. These departures can often be characterized by introducing a hypothetical filter as shown in Fig. 2*b*, which accounts for the departures from the ideal. The output from the real system can be written as

$$\begin{aligned} \hat{e}_o(f) &= H_{\text{dep}}(f)\,\hat{e}_{oi} \\ &= H_{\text{dep}}(f)\,H_{\text{ideal}}(f)\,\hat{e}_i(f) \end{aligned} \tag{8}$$

The product $H_{\text{dep}}(f)H_{\text{ideal}}(f)$ is thus the real response of the analog, $H_{\text{real}}(f)$. Thus the frequency response function of the departure from ideal can be determined as

$$H_{\text{dep}}(f) = H_{\text{real}}(f)/H_{\text{ideal}}(f) \tag{9}$$

Since, in general, the frequency response function is complex, the departures from ideal can be in both the amplitude and phase.

The effect of attenuating the higher Fourier components by a rolloff in the amplitude response is generally well understood. The effect of phase errors can be much more difficult to assess because, in effect, some Fourier components are delayed with respect to others so that the waveforms are distorted. *An important exception occurs when the phase errors vary linearly with frequency*, in which case all Fourier components are delayed by a fixed time delay and no distortion occurs.

Figures 3*a* and 3*b* show the amplitude and phase characteristics of the Q-meter design due to Oldfield et al [9]. As shown in the preceding section, it is the departure frequency response function which is primarily of interest here. Figures 4*a* and 4*b* plot the amplitude and phase characteristics of the departure. The linear-linear plot of the amplitude in Fig. 4*a* makes it clear that there is considerable attenuation at frequencies well below the half-power points, a fact often obscured by the usual log-log plots. It is also clear from both Figs. 3*b* and 4*b* that the Q-meter does not produce the desired 45° phase shift. Fortunately, however, the phase shift is linear with frequency below the half-power point (~ 100 kHz). As pointed out earlier, this means that the individual Fourier components are *not* shifted with respect to each other but the entire signal is delayed by an amount $A/2\pi$ where A is the constant of proportionality between the phase shift Δ and the frequency f. The lag for the circuit shown is ~ 4 μs. Note that even this linear phase shift can pose a problem when more than one gauge is to be used to obtain cross-spectral information if the phase characteristics of all Q-meters are not the same.

Figures 5 and 6 show the effect of the departures from ideal on two typical heat flux signals. Figure 5 shows the response of the analog to a square wave with a fundamental frequency of 13 kHz. Figure 6 shows the response of the analog to a pulse train with fundamental frequency also chosen at 13 kHz and pulse width equal to one-seventh of the period. Unlike the square-wave response, which is reasonable, the pulse train shows considerable distortion because of the removal of the harmonics by the finite bandwidth of the analog. Without some careful thought about the representative Fourier series for the pulse train, it might have been very difficult to have guessed the real waveform from the analog

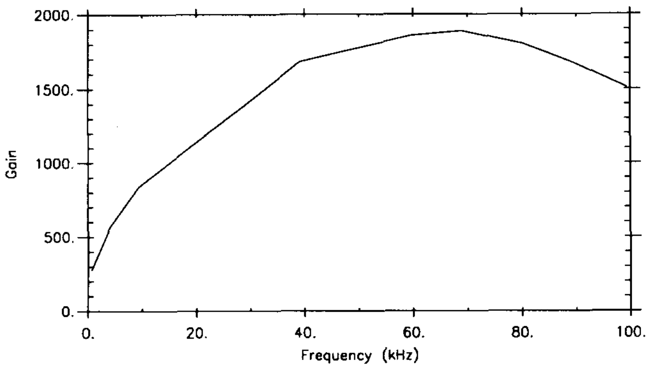

(a)

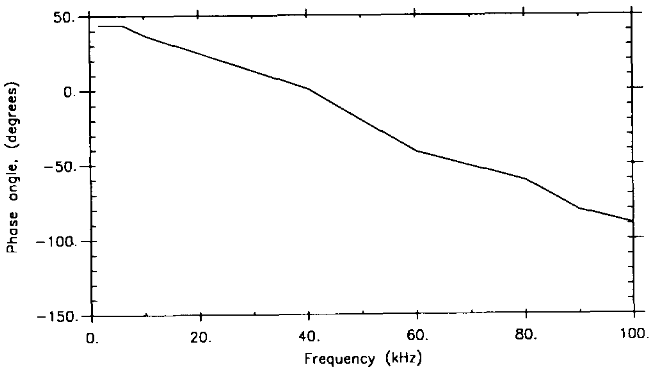

(b)

Figure 3. (a) Gain characteristic for Q-meter [9]. (b) Phase characteristic for Q-meter [9].

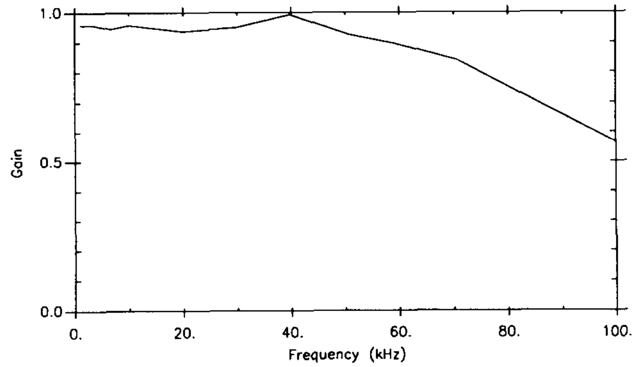

(a)

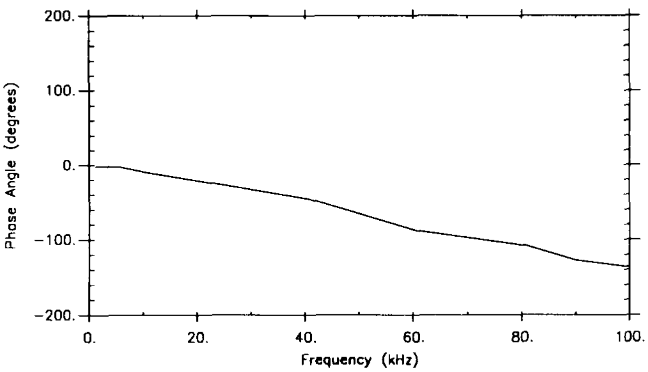

(b)

Figure 4. (a) Gain characteristic for difference from ideal response. (b) Phase chracteristic for difference from ideal response.

output, especially in view of the negative regions of the signal. Thus the importance of knowing the frequency response of the system cannot be underestimated if the original waveform is to be determined.

A MODEL FOR THE UNSTEADY TEMPERATURE SIGNAL

The unsteady temperature signal from a thin-film gauge on the rotor of a turbine blade in a transient test facility (in this case a shock tunnel) is shown in Fig. 7. The rapid rise in temperature is associated with the arrival of the test gas and marks a step change in the heat flux. The temperature signal rises with an approximately $t^{1/2}$ dependence because of the heat transfer to the substrate. Superimposed on the overall rise are the fluctuations resulting from the vane–wake crossings and other unsteady effects in the flow.

One of the difficulties in testing either analog circuits or numerical algorithms is the difficulty in generating a known temperature input signal which possesses the characteristics of a transient experiment like that described above. A particularly useful choice for a test signal would be one which yields a step change in heat flux (corresponding to the test initiation in a transient facility) superimposed on which is a sinusoidally oscillating unsteady heat flux. Such a heat flux signal is given by

$$q(0,t) = A_0 + A_1 \cos 2\pi f_0 t + B_1 \sin 2\pi f_0 t \quad \textbf{(10)}$$

where f_0 is a given frequency and where A_0, A_1, and B_1 are arbitrarily chosen coefficients. This is shown in Fig. 8*a* and corresponds to a single Fourier component plus the dc part of the signal which might be seen in a transient facility. If the temperature signal which produces such a heat flux

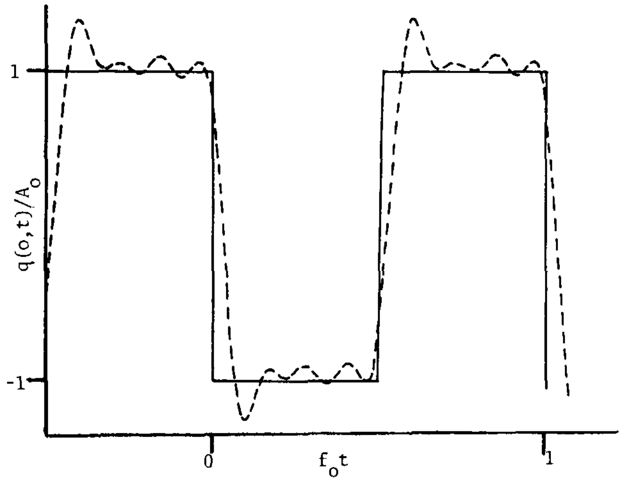

Figure 5. Response of Q-meter to input which would ideally generate a square-wave output.

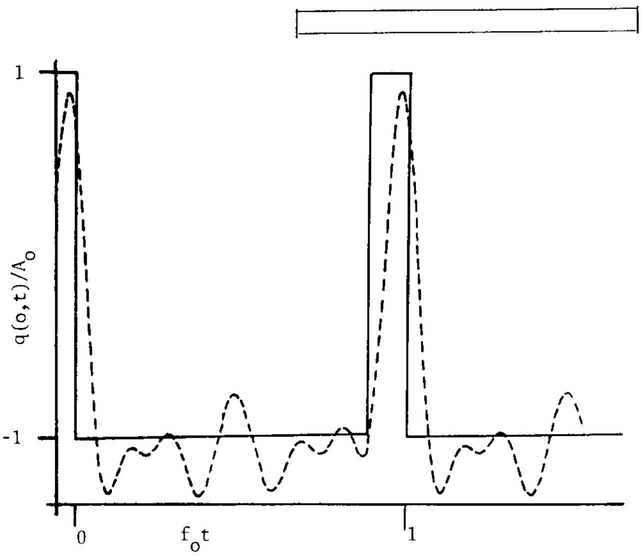

Figure 6. Response of Q-meter to input which ideally generates a pulse train output.

could be determined, it could be utilized to test numerical algorithms designed to directly calculate the heat flux from the measured surface temperature.

For constant thermal properties and zero film thickness, Eqs. (1) and (2) can be solved analytically to yield (Vidal [1])

$$T(0,t) = \frac{1}{\sqrt{\pi\rho Ck}} \int_0^t \frac{\dot{q}(0,\lambda)}{\sqrt{t-\lambda}}\, d\lambda + T_0 \quad \textbf{(11)}$$

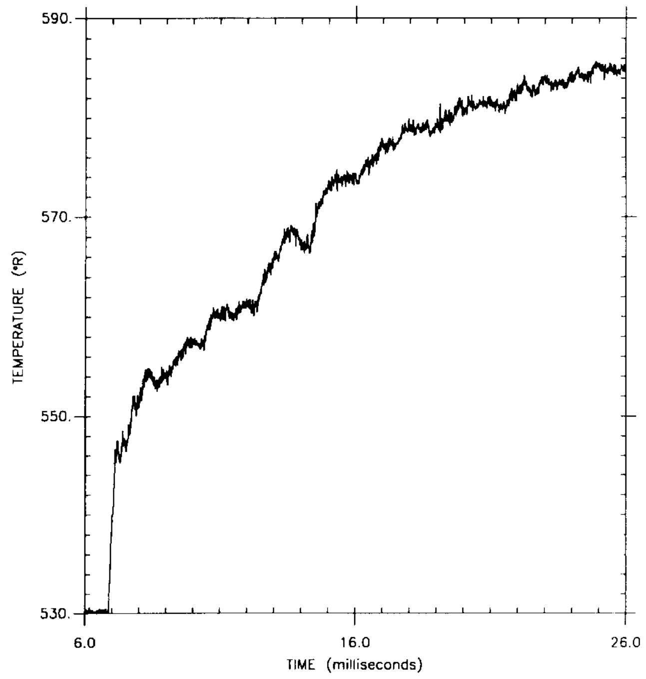

Figure 7. Typical surface temperature measured by thin-film gauge on turbine rotor in a shock tunnel.

Substitution of Eq. (10) into Eq. (11) yields, after integration,

$$\begin{aligned} &\sqrt{2\pi f_0}\,\frac{\sqrt{\pi\rho Ck}}{A_0}\,T(0,t) \\ &\quad = \sqrt{8\pi f_0 t} + \sqrt{2\pi} \\ &\qquad \times \left\{ C(2\pi f_0 t)\left[\frac{A_1}{A_0}\cos 2\pi f_0 t + \frac{B_1}{A_0}\sin 2\pi f_0 t\right] \right. \\ &\qquad \left. + S(2\pi f_0 t)\left[\frac{A_1}{A_0}\sin 2\pi f_0 t + \frac{B_1}{A_0}\cos 2\pi f_0 t\right]\right\} \quad \textbf{(12)} \end{aligned}$$

where

$$C(u) = \frac{1}{\sqrt{2\pi}} \int_0^u \frac{\cos\alpha}{\sqrt{\alpha}}\, d\alpha \quad \textbf{(13)}$$

and

$$S(u) = \frac{1}{\sqrt{2\pi}} \int_0^u \frac{\sin\alpha}{\sqrt{\alpha}}\, d\alpha \quad \textbf{(14)}$$

The integrals $C(u)$ and $S(u)$ can be recognized as the familiar Fresnel integrals (Abramowitz and Stegun [12]). Figure 8*b* shows the temperature variation which would produce the heat transfer signal corresponding to $A_1 = 0$, $B_1/A_0 = 1/4$. Because the Fresnel integrals in Eq. (12) can

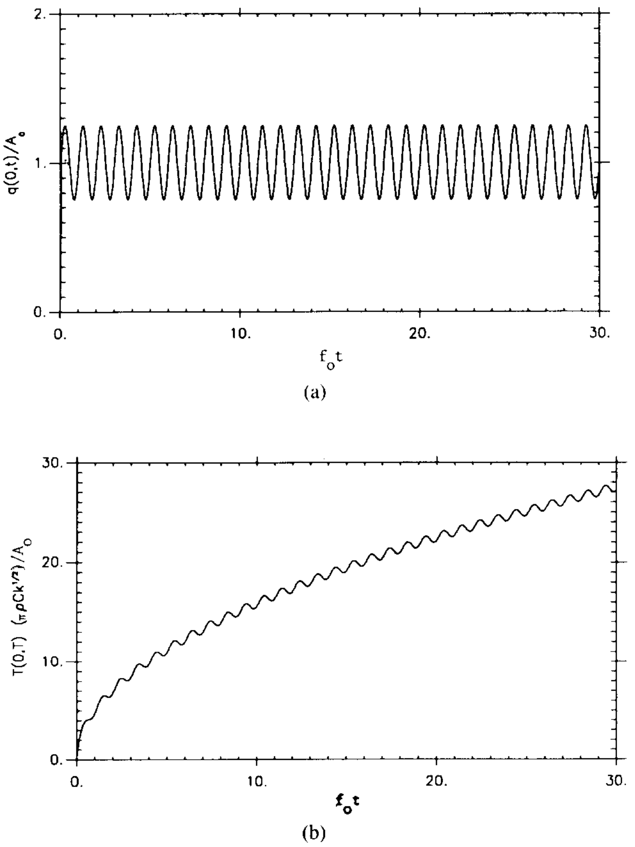

Figure 8. (a) Step rise in heat flux plus sinusoidal oscillation $[A_1/A_0 = 0,\ A_1/A_0 = 1/4$ in Eq. (10)]. (b) Response of surface temperature to heat flux in (a).

be evaluated by a variety of convenient formulas, the temperature history of Eq. (12) is particularly useful for testing finite-difference algorithms for solving Eq. (1) with unsteady inputs. It can also be used to evaluate the overall phase and amplitude response of the data processing system if the impulse response function of the system is known.

Before using the Fresnel-integral temperature history, it is interesting to look at the asymptotic behavior of Eq. (12). It is straightforward to show by using the asymptotic expansions of the integrals C and S (Abramowitz and Stegun [12]) that for $2\pi f_0 t \gg 1$,

$$\sqrt{2\pi f_0}\,\frac{\sqrt{\pi\rho Ck}}{A_0}\,T(0,t) = \sqrt{8\pi f_0 t}\left\{1 + \frac{\sqrt{2\pi}}{\sqrt{8\pi f_0 t}}\right.$$
$$\times\left[\frac{1}{2} + \frac{\gamma\sin 2\pi f_0 t}{\sqrt{2\pi f_0 t}} + \cdots\right]$$
$$\times\left[\frac{A_1}{A_0}\cos 2\pi f_0 t + \frac{B_1}{A_0}\sin 2\pi f_0 t\right]$$
$$+\left[\frac{1}{2} - \frac{\gamma\cos 2\pi f_0 t}{\sqrt{2\pi f_0 t}} + \cdots\right]$$
$$\left.\times\left[\frac{A_1}{A_0}\sin 2\pi f_0 t - \frac{B_1}{A_0}\cos 2\pi f_0 t\right]\right\} \qquad (15)$$

The neglected terms are of order $(2\pi f_0 t)^{-1}$, and the expansion is valid for $2\pi f_0 t > 40$ (or after about six cycles).

The $t^{1/2}$ dependence can be recognized as the surface temperature rise due to a step change in heat flux applied to a semi-infinite slab. Of particular interest to the experimentalist is the fact that the ratio of the fluctuating part of the temperature to the $t^{1/2}$ rise is continuously reduced with time. This makes it very difficult to directly sample the film temperature signal without burying the fluctuating part in the quantization noise of the A/D converter. The Q-meter with its $\sqrt{f}$ response tends to alleviate this problem, as does the differentiation approach of Dunn et al [5].

In the following section the Fresnel integral temperature history will be used to evaluate several numerical schemes for directly evaluating the heat flux from the surface temperature. Of particular interest will be the amplitude and phase errors introduced by the algorithms. Such an evaluation will be possible because the actual heat flux is known to be that given by Eq. (10).

NUMERICAL ALGORITHMS FOR CALCULATING HEAT FLUX FROM SURFACE TEMPERATURE MEASUREMENTS

An alternative to the analog Q-meter is the direct calculation of heat flux from the time-dependent surface temperature measured by the gauge. For all but the simplest inputs (and then only if the thermal properties are assumed constant), the solutions to Eqs. (1) and (11) cannot be obtained in closed form and must be calculated numerically. The particular problem here falls into the general class of inverse heat conduction and ill-posed problems for which there is an extensive literature. (Beck et al [13] provide an excellent summary of both examples and pitfalls of the various numerical approaches.) This paper will consider two numerical algorithms which have been used for processing thin-film gauge data: the first, the finite-difference approximation to the exact solution for constant thermal properties proposed by Cooke and Felderman [10], and the second, the simple implicit scheme for variable thermal properties used by Dunn et al [5]. The focus of the evaluation here will be on the ability of the algorithms to faithfully represent the amplitude and phase of rapidly varying input data and on their sensitivity to the quantization errors and noise encountered in typical applications.

The Cooke–Felderman Algorithm This algorithm is based on the integral solution to Eqs. (1) and (2) for constant thermal properties, which is

$$q(0,t) = \left(\frac{\rho Ck}{\pi}\right)^{1/2}\left[\frac{T(0,t)}{\sqrt{t}} + \frac{1}{2}\int_0^t \frac{[T(0,t) - T(0,\lambda)]}{(t-\lambda)^{3/2}}\,d\lambda\right] \qquad (16)$$

The first numerical approximation to Eq. (16) was proposed by Vidal [1], who used it to calculate heat flux from thin-film gauges in shock tunnels. Cooke and Felderman [10] improved Vidal's algorithm by approximating the temperature in Eq. (16) at time steps Δt with a piecewise linear signal. The results for the nth realization of the surface heat flux ($t = n\text{th}\,\Delta t$) is given by

$$q_n = \left(\frac{\rho Ck}{\pi}\right)^{1/2} 2(\Delta t)^{-1/2} \times \sum_{i=1}^{n} \frac{T_i - T_{i-1}}{(n-i)^{1/2} + (n-i+1)^{1/2}} \qquad (17)$$

In spite of its obvious advantage over a finite-difference solution, Eq. (17) is valid only if the thermal properties are constant. Moreover, whereas it has received extensive use in the calculation of heat fluxes in transient environments, the ability of this algorithm to accurately reproduce rapidly varying fluctuations in the unsteady heat flux has not been established.

If the effects of variable thermal properties on the instantaneous heat flux are to be accounted for, there appears to be no alternative to solving the heat conduction equation numerically. (Note, however, that corrections to Eq. (17) for varying thermal properties have been proposed by Miller [14].) Dunn et al [4] proposed a technique utilizing a Crank–Nicolson finite-difference procedure. Unfortunately, the equations were cast in terms of the similarity variable $\eta = x/\sqrt{\alpha t}$, which rendered the solution incapable of following rapid fluctuations at large time because of the increasing grid spacing. The problem encountered above has been reported in detail in Dunn et al [5]. However, because of its importance to the problem of resolving fluctuating heat transfer rates, it will be briefly summarized here.

When the heat transfer rate contains a part that fluctuates at frequency ω,* a second scale enters the problem—namely $\sqrt{\alpha/\omega}$, which is properly called the skin depth and is independent of time. The classical solution of a sinusoidal surface temperature variation (Carslaw and Jaeger [15]) contains an early-time transient plus the solution:

$$\Delta T(x,t) = A \exp\{-x\sqrt{\omega/\alpha x}\} \cos\{\omega t - x\sqrt{\omega/\alpha}\} \tag{18}$$

Thus the high-frequency portion of the surface temperature rise has a very shallow penetration, and care must be taken in the numerical work to resolve this thin layer properly. Solutions of Eq. (1) which use a fixed step size in the η direction will have a small value of Δx at early time and a large one at late time. Clearly the solution is to avoid the problem by differencing in x, not η.

Dunn et al [5] proposed a simple-implicit algorithm given by

$$\frac{\phi(i,j+1)-\phi(i,j)}{t_{j+1}-t_j} = \alpha(x_j, t_j) \times \frac{\phi(i+1,j+1)-2\phi(i,j+1)+\phi(i-1,j+1)}{(\Delta x)^2} \tag{19}$$

where ϕ is defined by the Kirchhoff transformation (see Carslaw and Jaeger [15]) by

$$\phi \equiv \int_{T_{\text{ref}}}^{T} \frac{k}{k_{\text{ref}}}\, dT \tag{20}$$

This equation was solved on a grid of variable size. At every time step, the boundary condition of zero temperature rise was enforced at a depth of $7\sqrt{\alpha_{\text{ref}} t}$. The heat transfer rate was found from a second-order accurate expression for the derivative at the surface.

Implicit numerical procedures for solving Eq. (15) work best when the step-size ratio

$$r = \alpha \Delta t/(\Delta x)^2 \tag{21}$$

is in the range 0.25–0.5 [16]. It happens that this criterion can be met for the test conditions of interest here by taking the sampling interval Δt on the basis of the Nyquist criterion to be inversely proportional to the highest frequency of interest, that is, $\Delta t \sim \pi/\omega \sim 1/2f$. The spatial step size Δx must be small enough to resolve the skin depth; that is, $\Delta x \leq \sqrt{\alpha/\omega}$. A constant value of the step-size ratio r will satisfy both of these criteria.

EVALUATION OF NUMERICAL ALGORITHM

The purpose of this section is to evaluate the algorithms outlined above by using the Fresnel-integral temperature proposed earlier. Of special concern to the experimentalist are the rate at which data must be taken relative to the frequencies of interest and the sensitivity of the algorithms to noise on the sampled signal or introduced by the sampling process.

Digital temperature data were generated using the Fresnel-integral temperature given by Eq. (12) and shown in Fig. 8*b*. These data were sampled at rates of 3.75, 7.5, 15, and 30 times the fundamental and then used as input to the numerical algorithms.

Figures 9–12 demonstrate the relative abilities of the Cooke–Felderman algorithm of Eq. (17) and the simple implicit scheme of Eq. (19). Note that the progressively poorer reconstruction of the sine wave part of the signal with decreasing number of points per cycle is due to the fact that the graphs have been produced using straight line segments, a procedure generally requiring about 10 points per cycle to produce a smooth sinusoidal curve. Of more concern here are the magnitude and phase errors of the computed heat flux signals relative to the exact signals. It is clear from the figures that both algorithms suffer from a slight phase lag (about 20°) for the lowest sampling rate (Fig. 12). This has virtually disappeared for the Cooke–Felderman algorithm when the sampling rate has increased to $f_s/f_0 = 15$ (Fig. 10) but persists to even $f_s/f_0 = 30$ (Fig. 9) for the simple implicit algorithm. Figure 13 shows how the relative magnitudes of the sinusoidal part of the signal vary with the sampling rate. The Cooke–Felderman algorithm slightly overpredicts the peaks, whereas the simple implicit scheme underpredicts them. Both algorithms converge toward the correct amplitude as the sampling rate increases.

In order to assess the sensitivity to noise on the input data, a second set of input data was generated by truncating the digital word size of the input data to a single byte. The effect is to introduce a quantization noise on the signal which is the same as if it had been sampled by an 8-bit A/D converter. (Note this is a relatively large amount of noise, since most A/D converters that would be employed for unsteady signal measurement are 10 bits or greater.) Figure 14*a* shows a

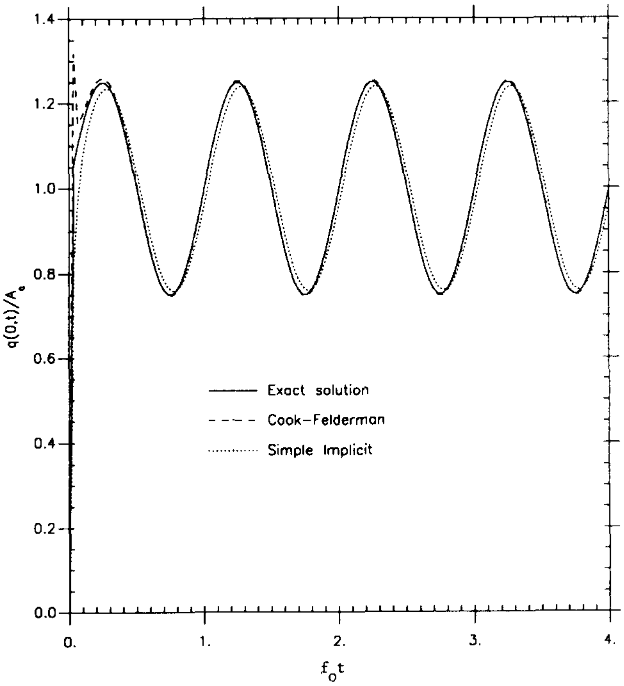

Figure 9. Computed response to Fresnel-integral temperature ($f_s f_0 = 30$).

* The radial frequency $\omega = 2\pi f$ is used here for convenience.

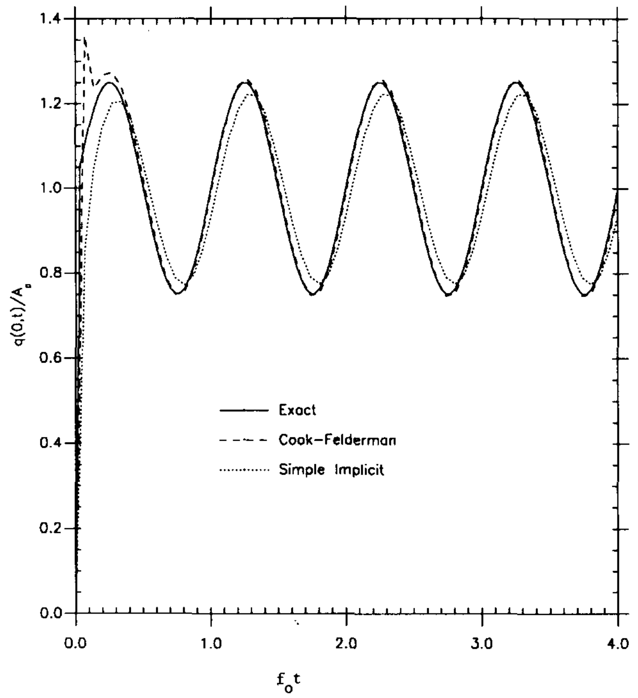

Figure 10. Computed response to Fresnel-integral temperature ($f_s/f_0 = 15$).

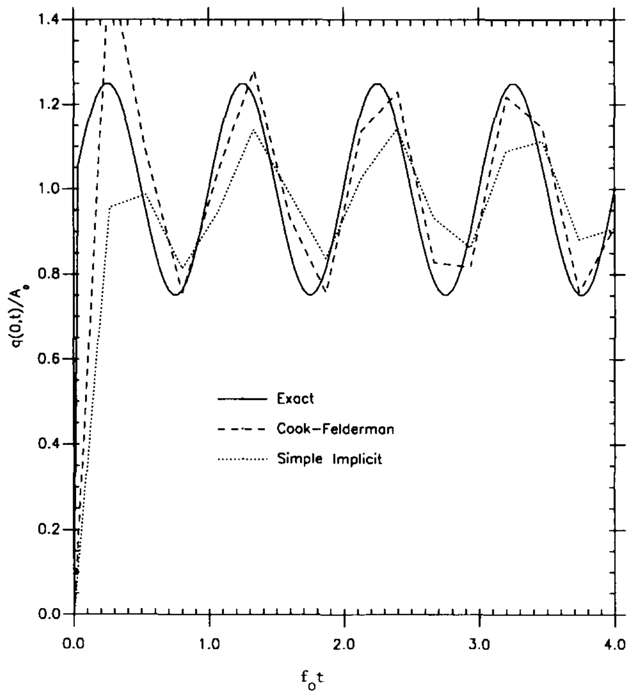

Figure 12. Computed response to Fresnel-integral temperature ($f_s/f_0 = 3.75$).

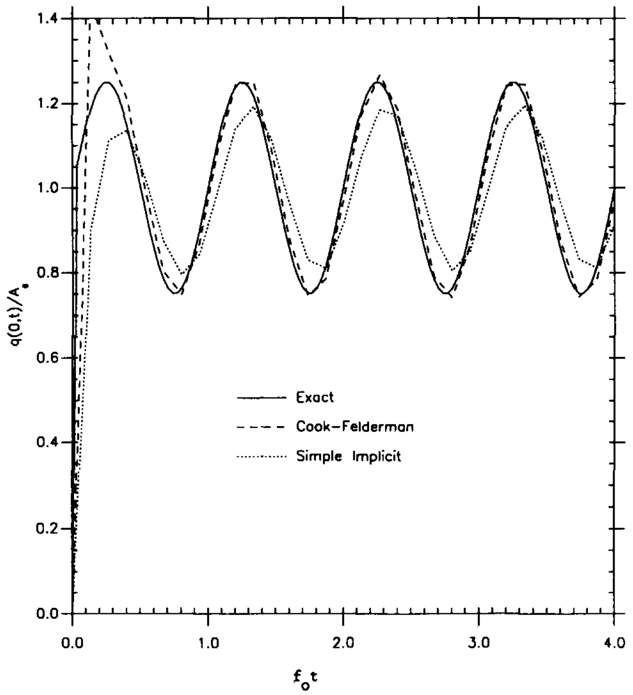

Figure 11. Computed response to Fresnel-integral temperature ($f_s/f_0 = 7.5$).

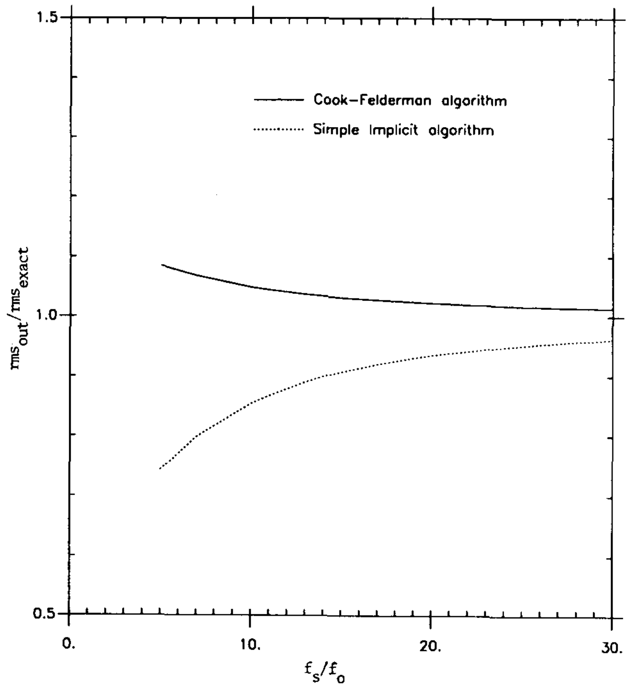

Figure 13. Ratio of computed rms output to root mean square of exact solution.

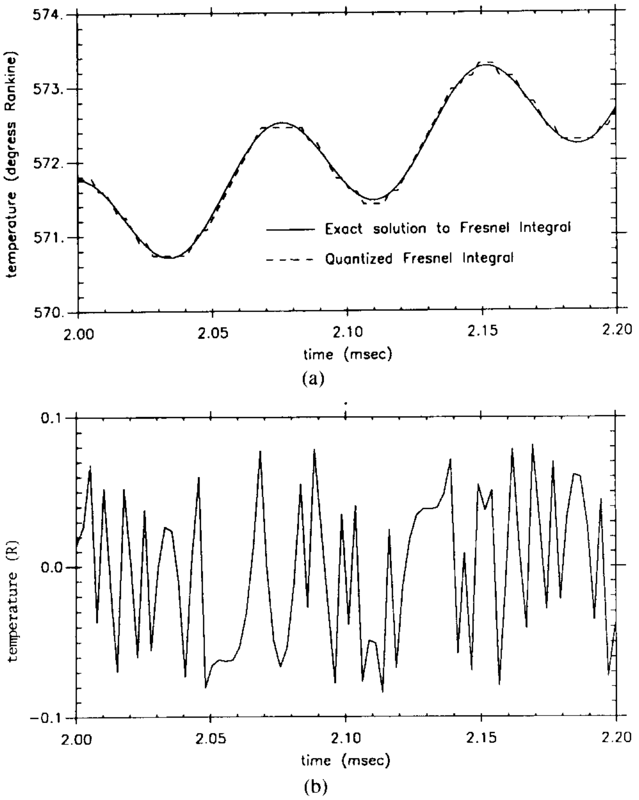

Figure 14. (a) Typical Fresnel-integral temperature input with and without 8-bit quantization. (b) Difference between exact and quantized Fresnel-integral temperatures in (a).

typical quantized input signal, while Figure 14*b* shows the difference between quantized and original input signal. The "noise level" is most easily characterized by defining ϵ to be the ratio of the size of the quantized step to the peak-to-peak fluctuating part of the temperature. For the case shown here and in the subsequent applications, $\epsilon \simeq 0.012$.

Figures 15*a–d* show the effect of the 8-bit quantization on the Cooke–Felderman algorithm for the four sampling rates. These can be compared to the simple implicit results shown in Figs. 16*a–d*. Both algorithms show a slight increase in the noise present on the signal with increasing sampling rate. The simple implicit algorithm, however, is less sensitive to noise than is the Cooke–Felderman. This can probably be attributed to its poorer frequency response, which effectively low-pass filters the quantization noise.

SUMMARY AND CONCLUSIONS

The use of thin-film gauges for the measurement of unsteady heat transfer in transient facilities has been briefly reviewed, with particular attention to how the heat transfer is determined from the film temperature. The removal of Fourier components by the finite frequency response of analog Q-meters was shown to have a significant effect on the heat transfer inferred. Similarly, the sampling rate and choice of computational algorithm were shown to introduce similar problems for the numerical reconstruction of the unsteady heat transfer from the digitally sampled film temperature. The digital methods have the advantage that they require less hardware and can easily include the effects of the temperature-dependent thermal properties of the substrate.

The fundamental frequency limitations of thin-film gauges have not been discussed but will be mentioned briefly here. The upper frequency limit is proportional to $(\alpha_f/d^2)^{1/2}$, where α_f is the thermal diffusivity of the film itself and d is its thickness [2]. This is typically of order 10^6 Hz and is therefore well above the bandwidth of most applications. The principal determinant of the lowest frequency which can be measured is the penetration depth, which must be small compared to the size of the film so that the heat transfer into the substrate is effectively one-dimensional. Thus, if l is the smaller of the gauge dimension and the depth of the substrate, the lower cutoff frequency is of order $(\alpha/l^2)^{1/2}$, where α is the thermal diffusivity of the substrate, [2]. Analog Q-meters can deviate from the $f^{1/2}$ response at substantially higher frequencies because of design limitations. It is easy to see that these lower frequency limits place an upper limit on the duration of the test in transient facilities—at least the duration for which the determination of heat flux by the methods discussed here will be valid.

Finally, it should be noted that there are situations where thin-film gauges can be used for the measurement of periodic or statistically stationary heat flux measurement. [We are grateful to P. Magari and Professor J. LaGraff of Syracuse University for pointing this out to us.] The first of these is when the average heat flux is identically zero, in which case the transient part of the solution given by Eq. (15) dies off and only the periodic component remains. Then Eq. (3) can be applied directly to the unsteady part of the temperature signal to obtain spectra of the heat flux. This presumes, of course, that the lowest frequencies of interest are above the low-frequency cutoff described above and that the thermal properties are nearly constant. The second situation arises when the transient part of the temperature signal contributes only below the cutoff frequency, so that the unsteady part of the signal is not contaminated by it. In this case, the average heat transfer cannot be determined, but Eq. (3) can still be shown to be valid for the unsteady heat flux determination.

The research reported in this paper was supported by the National Aeronautics and Space Administration, Lewis Research Center, Cleveland, Ohio, under grants number NAG 3-469 and NAG 3-581. The work was a part of the CUBRC Gas Turbine Research Program under the direction of Dr. Michael Dunn, to whom we are indebted for his encouragement and technical insights. The contributions of Paul Seymour and James Sonnenmeier are also gratefully acknowledged.

An earlier version of this paper was presented at the 1987 ASME-JSME Thermal Engineering Joint Conference and published in the proceedings thereof (George et al [17]).

We are grateful to Dr. Martin Oldfield of Oxford University and Dr. James O'Brien of NASA/Lewis for providing the data for Figs. 3 and 4.

NOMENCLATURE

A_0	dc part of unsteady heat flux signal, W/m^2
A_1	coefficient in Eq. (10), W/m^2
B_1	coefficient in Eq. (10), W/m^2
C	thermal capacity, J/(kg · K)
$C(u)$	Fresnel integral, see Eq. (13), dimensionless
d	film thickness, m
$\hat{e}_i$	Fourier transform of input voltage, V · s
$\hat{e}_{oi}$	Fourier transform of ideal output voltage, V · s
$\hat{e}_o$	Fourier transform of real output voltage, V · s
H_{dep}	defined by Eq. (9), dimensionless
f	frequency, Hz
H_{ideal}	frequency response function of ideal system, dimensionless

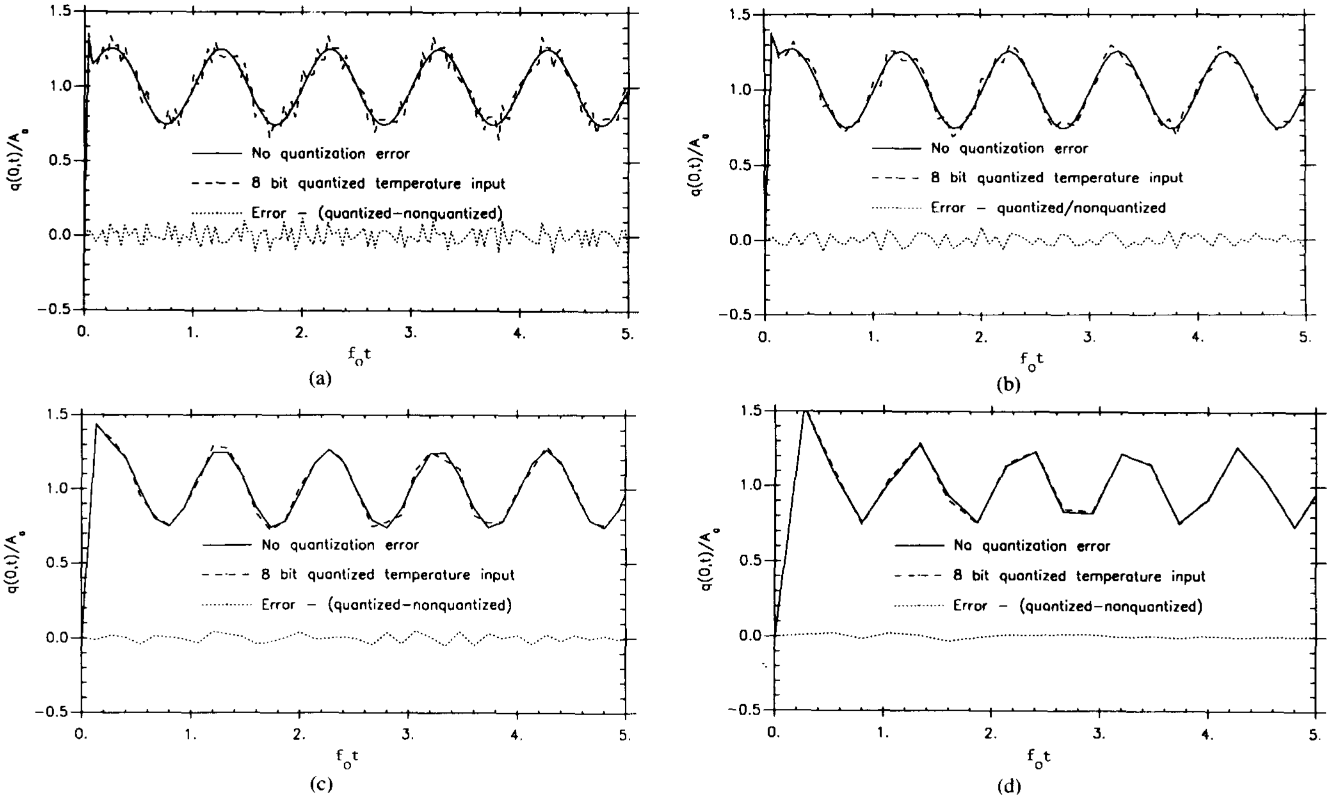

Figure 15. Sensitivity of Cook–Felderman algorithm to quantization noise on input. (a) $f_s/f_0 = 30$, $\epsilon = 0.12$; (b) $f_s/f_0 = 15$, $\epsilon = 0.12$. (c) $f_s/f_0 = 7.5$, $\epsilon = 0.12$; (d) $f_s/f_0 = 3.75$, $\epsilon = 0.12$.

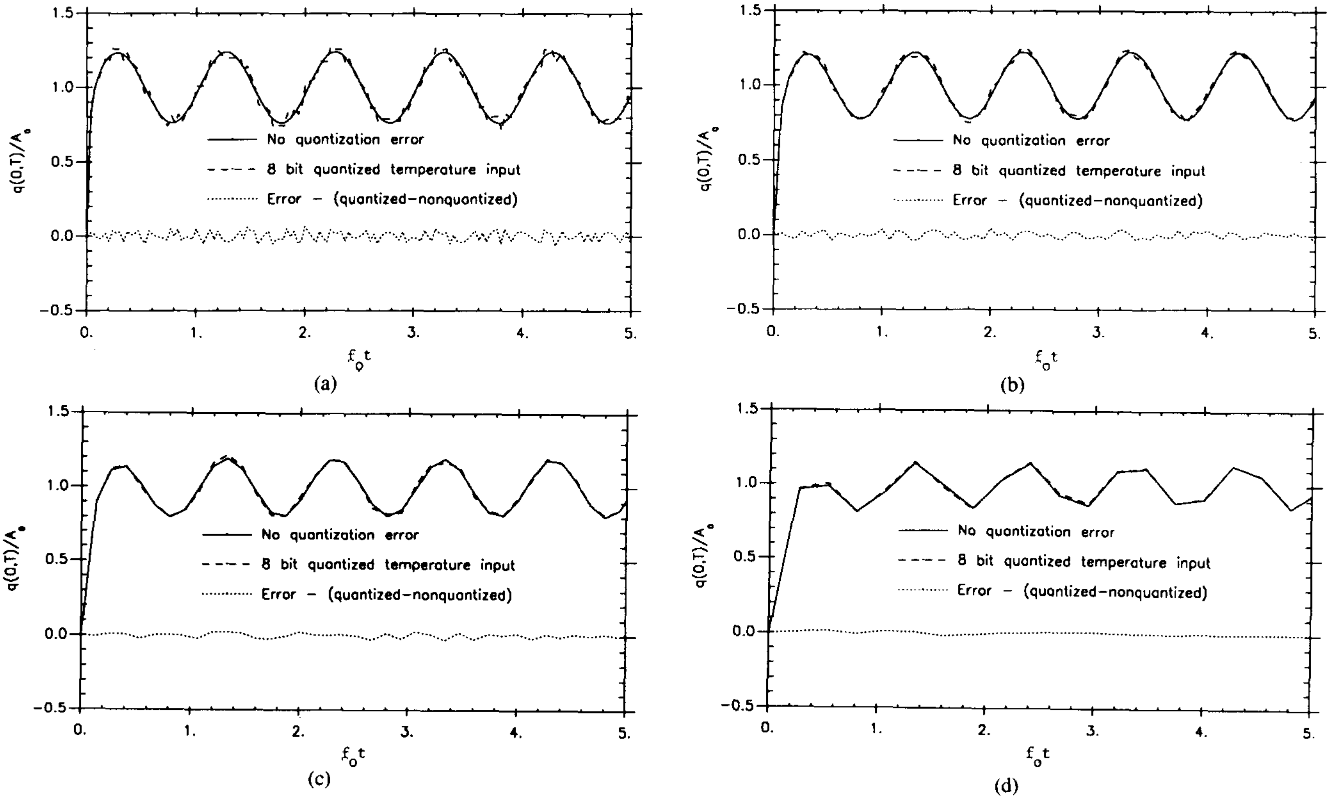

Figure 16. Sensitivity of simple implicit algorithm to quantization noise on input. (a) $f_s/f_0 = 30$, $\epsilon = 0.12$; (b) $f_s/f_0 = 15$, $\epsilon = 0.12$. (c) $f_s/f_0 = 7.5$, $\epsilon = 0.12$; (d) $f_s/f_0 = 3.75$, $\epsilon = 0.12$.

H_{real} frequency response function of real system, dimensionless
k thermal conductivity, W/m
l smallest lateral dimension of film, or depth of substrate, m
$\dot{q}$ heat flux, W/m^2
q Fourier transform of $\dot{q}$, $W \cdot s/m^2$
$S(u)$ Fresnel integral, see Eq. (14), dimensionless
T temperature of gauge, K
$\hat{T}$ Fourier transform of T, $K \cdot s$
t time, s
x coordinate in substrate (Fig. 1), m

Greek Symbols

α thermal diffusivity of substrate, m^2
α_f thermal diffusivity of film, m^2
γ constant (= 0.3989), dimensionless
Δt time between samples, Eqs. (17)-(21), s
ϵ ratio of quantization step to peak-to-peak signal, dimensionless
λ integration variable (time), s
ρ density of substrate, kg/m^3

REFERENCES

1. Vidal, R. J., Model Instrumentation Techniques for Heat Transfer and Force Measurements in a Hypersonic Shock Tunnel, Cornell Aeronautical Laboratory Rept. M. AD-917-A-1, 1956.
2. Schultz, D. L., and Jones, T. V., Heat Transfer Measurements in Short Duration Hypersonic Facilities, AGARDograph No. 165, 1973.
3. Dunn, M. G., and Holt, J. L., Turbine Stage Heat Flux Measurements, AIAA/ASME 18th Joint Propulsion Conference, Cleveland, Ohio, June 21-23, Paper No. 82-1289, 1982.
4. Dunn, M. G., Rae, W. J., and Holt, J. L., Measurement and Analysis of Heat-Flux Data in a Turbine Stage. Part I. Description of Experimental Apparatus and Data Analysis, *J. Eng. Power*, **106**, 229-240, 1986.
5. Dunn, M. G., George, W. K., Rae, W. J., Woodward, S. H., Moller, J. C., and Seymour, P. J., Heat Flux Measurements for the Rotor of a Full-Stage Turbine. Part II. Description of Analysis Techniques and Typical Time Resolved Measurements, ASME 31st Int. Gas Turbine Conf., Dusseldorf, West Germany, 8-12 June, 1986.
6. Doorly, D. J., and Oldfield, M. L. G., Simulation of the Effects of Shock Wave Passing on a Turbine Rotor Blade, ASME Paper No. 85-GT-112, 1985.
7. Skinner, G. T., Analog Network to Convert Surface Temperature to Heat Flux, *J. Am. Rocket Soc.*, **30**, 569-570, 1960.
8. Meyer, R. F., A Heat Flux Meter for Use with Thin Film Surface Thermometers, NRC Canada Aero Rept. LR-279, 1960.
9. Oldfield, M. L. G., Burd, H. J., and Doe, N. G., Design of Wide-Bandwidth Analogue Circuits for Heat Transfer Instrumentation in Transient Tunnels, in *Heat and Mass Transfer in Rotating Machinery*, D. E. Metzger and N. Afgan, Eds., Hemisphere, New York, pp. 233-258, 1980.
10. Cook, W. J., and Felderman, E. J., Reduction of Data from Thin-Film Heat Transfer Gauges: A Concise Numerical Technique, *AIAA J.*, **4**(3), 561-562, 1966.
11. Cook, W. J., Determination of Heat-Transfer Rates from Transient Surface Temperature Measurements, *AIAA J.*, **8**(7), 1366-1368, 1970.
12. Abramowitz, M., and Stegun, I. S., *Handbook of Mathematical Functions*, Appl. Math. Ser. 55, National Bureau of Standards, Washington, D.C., 1964.
13. Beck, J. V., Blackwell, B., and St. Clair, C. R., Jr., Inverse Heat Conduction, III. Posed Problems, Wiley-Interscience, New York, 1985.
14. Miller, C. G., Comparison of Thin-Film Resistance Heat-Transfer Gages with Thin-Skin Transient Calorimeter Gages in Conventional Hypersonic Wind Tunnels, NASA TM 83197, 1981.
15. Carslaw, H. S., and Jaeger, J. C., *Conduction of Heat in Solids*, 2nd ed., Section 216, Clarendon Press, Oxford, 1960.
16. Anderson, J., Tannenhill, R., and Pletcher, R., *Computational Fluid Mechanics and Heat Transfer*, Hemisphere, New York, 1985.
17. George, W. K., Rae, W. J., Seymour, P. J., and Sonnemeier, J. R., An Evaluation of Analog and Numerical Techniques for Unsteady Heat Transfer Measurement with Thin Film Gauges in Transient Facilities, *Proc. ASME-JSME Engineering Joint Conference*, **2**, 611-617, 1987.

Received May 31, 1990; revised October 12, 1990